Systematics and empirical expressions for neutron emission from thick targets in α-induced reactions

Moumita Maiti and S. N. Roy
Department of Physics, Visva Bharati, Santiniketan-731235, India

Maitreyee Nandy
Saha Institute of Nuclear Physics, 1/AF, Bidhannagar, Kolkata-700064, India

P. K. Sarkar
H.P.U., V. E. C. Centre, 1/AF, Bidhannagar, Kolkata-700064, India
(Received 5 August 2004; published 15 March 2005)

The effect of two initial exciton (particle-hole) configurations, namely 4p0h and 5p1h, on the angular distribution of neutron emission from α-induced reactions on various thick targets have been analyzed. In the angular distribution of emitted neutrons the relative contribution of the 4p0h configuration is found to vary as the cosine of the angle of emission. Using such dependence, empirical expressions are developed for the total neutron yield, energy spectra, and angular distribution of neutrons in α-induced reactions in the 25–200-MeV energy range. These expressions are based on empirical fits to the hybrid model calculations of neutron emission from target elements in the mass range ^{9}Be to ^{209}Bi. The results of these calculations are compared with experimental data showing fairly good agreement. The empirical expressions provide a simple, fast, and reliable tool for calculating neutron emission essentially required for radiation shield design and other applications.

DOI: 10.1103/PhysRevC.71.034601 PACS number(s): 25.55.−e, 24.10.−i

I. INTRODUCTION

Nuclear reactions induced by α particles are complex in nature because this projectile is the lightest of the heavy ions and heaviest of the light ions retaining the features of both types. There are several mechanisms that have roles in α-induced reactions. Measurements of charged particle spectra from α-induced reactions on different nuclei have indicated the possibility of five different mechanisms by which an α projectile may be removed from the entrance channel. They are as follows:

(a) Inelastic scattering of incident α particles by the target nucleus as a whole. This leads to excitation of collective states above the particle emission threshold [1].
(b) Pickup reactions leading to creation of ^{5}He or ^{5}Li, followed by a breakup to a kinematically correlated α particle plus a nucleon [2].
(c) Binary fragmentation of the α particle [3–5].
(d) Dissolution of the α particle into four nucleons in the nuclear field [6,7].
(e) Interaction of the α particle with individual nucleons of the target nucleus, leading to a preequilibrium (PEQ) cascade of α-nucleon scattering.

The last three processes are more or less similar, because they lead to the destruction of the α particle and initiation of a PEQ cascade. As the first two mechanisms contribute of about 5% of the α-particle target nucleus interactions [8], they can be ignored to approximate the gross behavior of neutron emission from α-induced reactions.

In this work we confine our attention to only the last two reaction mechanisms that have major contributions to the total reaction cross section. They lead to, in the framework of exciton model analysis, two different initial configurations of the reaction process; 4 particle-0 hole (i.e., 4 excitons) because of process (d) and 5 particle-1 hole (6 excitons) because of process (e). It has been observed by Gadioli *et al*. [8] that 30% contribution from 4 particle-0 hole and 70% from 5 particle-1 hole reproduce the experimental results well in energy range of 25–200 MeV considered in the present work. We have calculated total neutron emission cross section using this assumption.

The main purpose of the present work is twofold. In the first place we intend to study the effect of the above two initial configurations on the emission angles of the PEQ neutrons in α-induced reactions. We do this by comparing experimentally measured neutron yield distributions at different angles from thick targets with those calculated using the ALICE91 [13,14] code based on exciton (hybrid) model. In an earlier work [9] an analysis of experimentally measured thick target neutron yield distributions from α-induced reactions was attempted using the same initial configurations in exciton (hybrid) model calculations. In that work the effect of the initial configurations on the angular distribution of emitted neutrons was not analyzed.

Our next intention is to formulate simple empirical relations for α-induced reactions to estimate neutron emission cross sections and thick target energy and angular distributions of emitted neutrons. The procedure adopted is outlined as follows. We have used the exciton (hybrid) model to calculate the required neutron emission data for various target elements and projectile energies. We have then used the least-squares fitting procedures to obtain simple polynomial expressions in a way

similar to what we had done earlier for proton projectiles [10]. In arriving at expressions for double differential neutron yield distributions we use the probabilities of initial configuration-mixing as obtained from the first part of our investigation. The final empirical relations will require only target mass and the projectile energy as input parameters to calculate the required quantities. Such simple relations will prove useful when incorporated in large scale Monte Carlo simulations of neutron yield from charged particle (e.g., high-energy proton) transport through targets of complex geometries and material compositions where α particles are generated as secondaries and produce neutrons in turn. Development of technologies related to accelerator-driven systems (ADS) puts a high premium on such large-scale computations. Further, thick target neutron yield from α-induced reactions can be used to approximate neutron yield from heavy-ion reactions [11].

In the next section we give a brief description of the ALICE91 code based on the exciton (hybrid) model and the modifications done to calculate thick target neutron yield. In Sec. III we compare the calculated results with the experimental data (thick target) on neutron distributions from α-induced reactions. We find out the proportion in which the results from 4p0h and 5p1h initial configurations are required to be combined to reproduce the experimental data. In Sec. IV we formulate the empirical relations of total neutron emission cross sections as well as total and differential neutron yield distributions from thick targets.

II. BRIEF DESCRIPTION OF THE HYBRID MODEL AND THE ALICE91 CODE

One of the commonly used nuclear reaction models for PEQ reactions is the hybrid model that combines the exciton model and the Boltzmann master equation (BME) approach to describe the PEQ reaction mechanism. In the framework of the hybrid model, relaxation of the target+projectile composite system proceeds through a cascade of two-body interactions when the excitation energy is shared between the interacting particles. Hybrid model [12] uses "never-come-back" approximation, that is, it assumes that particle-hole pairs may only be created at each stage of the relaxation process thus only increasing the number of excitons (n) present in it. Annihilation of a particle-hole pair or redistribution of energy among the excited particles are ignored. The model explicitly evaluates the preemission energy distribution of the ejectile at each stage n in terms of appropriate intermediate state densities. The total emission cross section for an ejectile of type x (neutron in our case) is given by the following:

$$\sigma^x_{\text{emission}} = \sigma^x_{\text{PEQ}} + \sigma^x_{\text{EQ}}, \tag{1}$$

where

$$\sigma^x_{\text{PEQ}} = \int_0^{\epsilon_{\max}} \sigma_{\text{PEQ}}(\epsilon_x) d\epsilon_x,$$
$$\sigma^x_{\text{EQ}} = \int_0^{\epsilon_{\max}} \sigma_{\text{EQ}}(\epsilon_x) d\epsilon_x, \tag{2}$$

σ^x_{PEQ} and σ^x_{EQ} are, respectively, the PEQ and equilibrium (EQ) emission cross section of the x-type nucleon, ϵ_x is the energy of the ejectile, and $\epsilon_{\max}$ is the maximum possible emission energy.

The PEQ emission probability is calculated from the preemission energy distribution of the ejectile and the emission probability. The emission rate is calculated from the rate of the reverse reaction and the total two-body interaction rate is given by an empirical formula [12] which takes into account the Pauli blocking effect. The hybrid model gives the PEQ emission cross section of a nucleon of type x as follows:

$$\begin{aligned}\sigma_{\text{PEQ}}(\epsilon_x) &= \sigma_{\text{abs}}(E_\alpha) \sum_{\substack{n=n_0,\\ \Delta n=2}}^{\bar{n}} P^H_n(\epsilon_x) \\ &= \sigma_{\text{abs}}(E_\alpha) \sum_{\substack{n=n_0,\\ \Delta n=2}}^{\bar{n}} D_n \left[{}_nX_x \frac{\rho_n(U,\epsilon_x)}{\rho_n(E_c)} \right] \frac{\lambda_c(\epsilon_x)}{\lambda_c(\epsilon_x) + \lambda_+(\epsilon_x)},\end{aligned} \tag{3}$$

where $P^H_n(\epsilon_x)$ is the hybrid model PEQ emission probability of x-type nucleon with energy ϵ_x from the n exciton state. $\sigma_{\text{abs}}(E_\alpha)$ is the absorption cross section of α in the target at incident energy E_α. D_n is the probability of reaching the n exciton state without prior emission and ${}_nX_x$ is the number of x-type excited nucleons in it. $\rho_n(E_c)$ is the partial level density of the n exciton state at excitation energy E_c. $\rho_n(U,\epsilon_x)$ is the partial level density of the same n exciton state with the same energy E_c distributed among n excitons in such a way that one particle-exciton has the energy $\epsilon_x + B_x$ and the rest $(n-1)$ excitons sharing the energy $U = E_c - \epsilon_x - B_x$, B_x being the separation energy of x. The ratio $\rho_n(U,\epsilon_x)/\rho_n(E_c)$ gives the probability of finding one x-type nucleon in the n exciton state with energy $\epsilon_x + B_x$ prior to emission. $\lambda_c(\epsilon_x)$ and $\lambda_+(\epsilon_x)$ are the emission and two-body interaction rate of x-type nucleon with energy ϵ_x respectively.

The EQ emission cross section is given by the following:

$$\sigma_{\text{EQ}}(\epsilon_x) \sim \sigma_{\text{comp}} \frac{e^{2(aU_r)^{1/2}}}{U_r}, \tag{4}$$

where σ_{comp} is the compound nucleus formation cross section, a is the level density parameter ($\propto A$), and U_r is the available excitation energy of the compound nucleus after PEQ emissions.

In the code ALICE91 [13,14] excitation energy of the composite nucleus up to 300 MeV can be considered. Single and simultaneous two-nucleon (n, p, nn, np, pp) PEQ emissions are considered but sequential multiple PEQ emissions are not calculated. ALICE91 does not have the provision for calculating PEQ emission of composite particles or clusters.

Evaporation calculations are done using a standard Weisskopf-Ewing formalism that reduces the computation time to 1% of that required for a detailed Hauser-Feshbach calculations. But it is done sacrificing rigor in physics. Evaporation of neutrons, protons, α's, and deuterons can be considered in ALICE91. Residual nuclei of a grid of 11 mass units wide and 9 atomic numbers deep may be calculated. The angular distribution of the emitted neutrons are calculated using the Kalbach systematics [15].

A. Thick target neutron yield distributions

In the present work we have chosen stopping targets, that is, the targets are thick enough so that the projectiles are completely stopped inside them. The emitted neutron spectrum from any such thick target is in reality a sum of all the spectra from continuously degrading projectile energies, starting from the incident energy down to the threshold energy for neutron emission from the target nucleus. The code ALICE91 has been modified to take into account this aspect.

In our calculations we have divided the target into a number of thin slabs, calculated the neutron emission spectrum from each slab, and summed them to obtain the total emitted spectrum. For a thin slab of thickness t the emitted spectrum $Y(E_\alpha, \epsilon, t)d\epsilon$ can be computed as follows:

$$Y(E_\alpha, \epsilon, t)d\epsilon = \sigma(E_\alpha, \epsilon)d\epsilon N t, \tag{5}$$

where N is the number of target atoms per unit volume, E_α is the incident α energy, and ϵ is the emitted neutron energy. The energy differential neutron emission cross section $\sigma(E_\alpha, \epsilon)d\epsilon$ is obtained from ALICE91 calculations. The thickness of each slab is so selected that the incident α loses a specified ΔE MeV energy in each slab. The kinetic energy of the projectile incident on the *ith* slab, E_α^i and the average energy $\bar{E}_\alpha^i$ in the *ith* slab are given, for a projectile of energy E_α^0 incident on the thick target by the following:

$$E_\alpha^i = E_\alpha^0 - (i-1)\Delta E, \tag{6}$$

$$\bar{E}_\alpha^i = \left(E_\alpha^i + E_\alpha^{i+1}\right)/2. \tag{7}$$

The slab thickness t_i is as follows:

$$t_i = \int_{E_\alpha^i}^{E_\alpha^{i+1}} \frac{dE}{-dE/dt}, \tag{8}$$

where dE/dt is the stopping power of α in the target material and it is calculated using the formalism of Ziegler *et al*. [16].

The total neutron yield $Y(E_\alpha, \epsilon)$ at energy ϵ is given by the following:

$$Y(E_\alpha, \epsilon)d\epsilon = \sum_{i=1}^{m} Y\left(\bar{E}_\alpha^i, \epsilon, t_i\right) \exp\left(-N\left[\sum_{k=1}^{i-1} \sigma_{\rm abs}\left(\bar{E}_\alpha^k\right) t_k\right]\right), \tag{9}$$

where $\sigma_{\rm abs}(\bar{E}_\alpha^k)$ is the absorption cross section of α of energy $\bar{E}_\alpha^k$ in the target element. Here, m is determined by $m = (E_\alpha^0 - E_\alpha^{th})/\Delta E$, where E_α^{th} is the α threshold energy for neutron production. For $i = 1$, the value of the exponential attenuation factor in Eq. (9) is taken to be unity. For the present calculations we have chosen $\Delta E = 1$ MeV.

B. Input details

In the present work neutron emission has been calculated using ALICE91 from residual nuclides (including the composite nucleus) 11 mass units wide and 9 charge units deep. Fermi gas level density is used to calculate neutron emission in the case of thick targets. The reaction cross section for the reverse channel is calculated using the optical model. Level density parameter is taken as $A/9$, which is the default option of the code. Weisskopf-Ewing formalism is used to estimate evaporation and angular distribution of emitted neutrons is calculated from Kalbach systematics. Two choices of initial exciton number 4p0h and 5p1h are used.

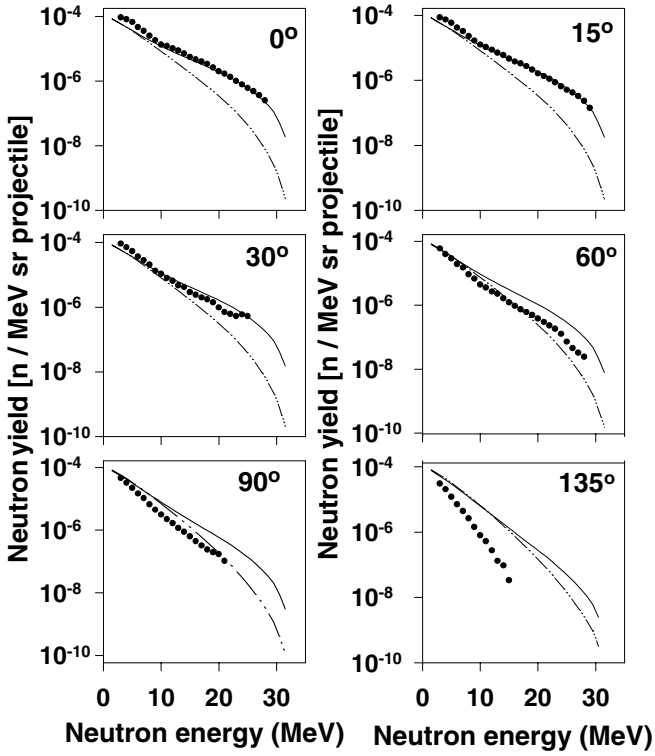

FIG. 1. Comparison of measured neutron yield (symbols) [21] for 40-MeV α on Al with calculated (modified ALICE91) results of 4p0h (solid lines) and 5p1h (solid-dot lines) initial configuration of α at six different angles.

III. ANGULAR DISTRIBUTION OF NEUTRONS FROM THICK TARGETS

The angular distribution of neutrons emitted from α-induced reaction on thick targets has been measured in several earlier works [17–20]. We now compare the experimentally obtained distributions with the neutron energy distributions at specified emission angles calculated in the framework of the hybrid model using ALICE91. The calculations are done, after carrying out the modification in the ALICE91 code as described in Sec. II, for the two different initial configurations: 4p0h and 5p1h. Figures 1–5 show the comparison between the experimental data and the calculated results for 40-MeV α on Al, Cu, Pb [21] targets as well as 50- and 60-MeV α on Ta [20]. From the plots it can be observed that the contribution to high-energy neutron emission is significantly higher for 4p0h initial exciton state than the 5p1h initial state. At forward angles (0°, 15°, and 30°) neutron distributions calculated with 4p0h initial configuration are very close to the experimental data. The 5p1h calculations underpredict the measured neutron distribution at higher emission energies at those angles. However, at larger angles, it can be seen that

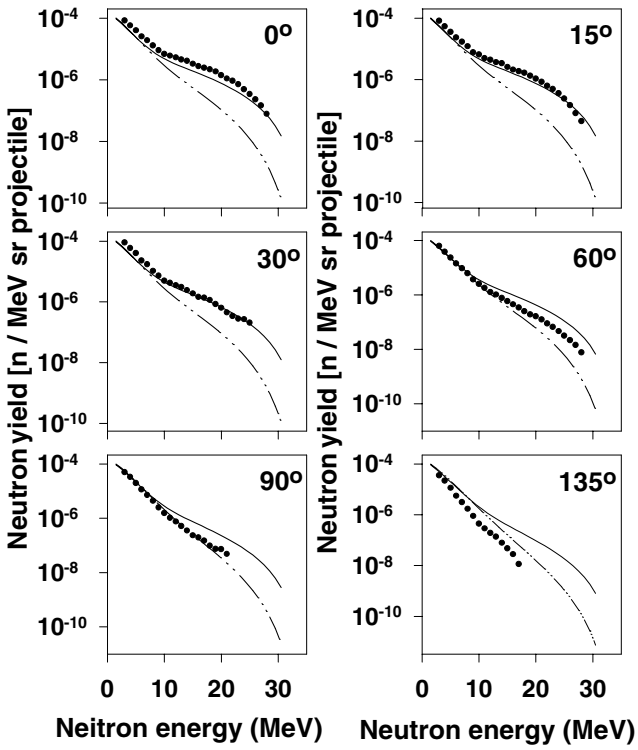

FIG. 2. Same as Fig. 1 for 40-MeV α on Cu.

up to 90° emission angle the experimental data are more closely predicted by the 5p1h calculations, whereas the 4p0h calculations begin to show overprediction compared to the measured data. These observations suggest that for α-induced reactions both the initial exciton configurations (4p0h and

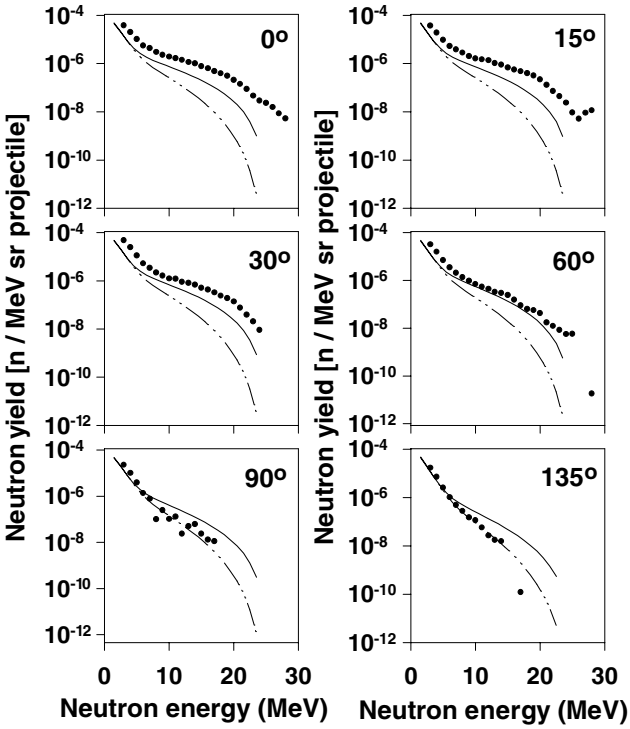

FIG. 3. Same as Fig. 1 for 40-MeV α on Pb.

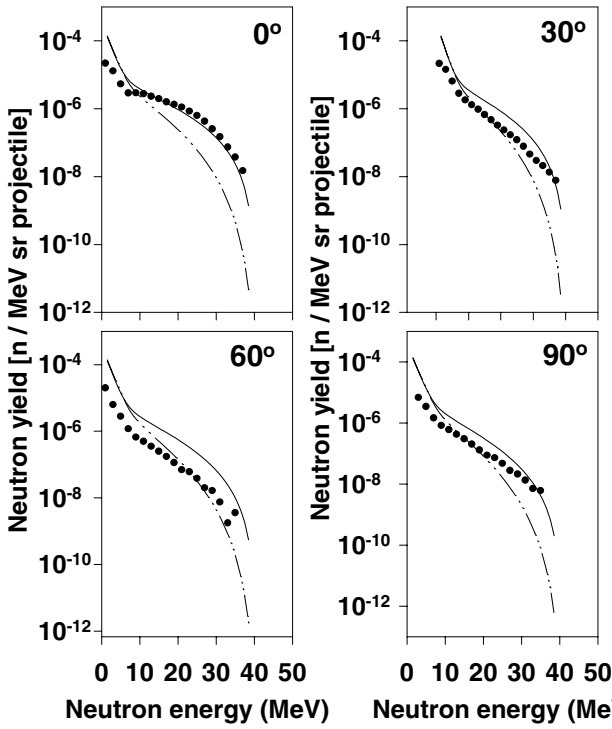

FIG. 4. Comparison of measured neutron yield (symbols) [20] for 50-MeV α on Ta with calculated (modified ALICE91) results of 4p0h (solid lines) and 5p1h (solid-dot lines) initial configuration of α at four different angles.

5p1h) have some proportional contribution to the directional distribution of neutrons, which depends on the emission angle θ. Our study reveals that for 0° to 90° emission angles, a multiplication factor of b (<1) for the 4p0h and $(1-b)$ for the 5p1h contributions might reproduce the angular distribution of the emitted neutrons. The factor b will be a function of

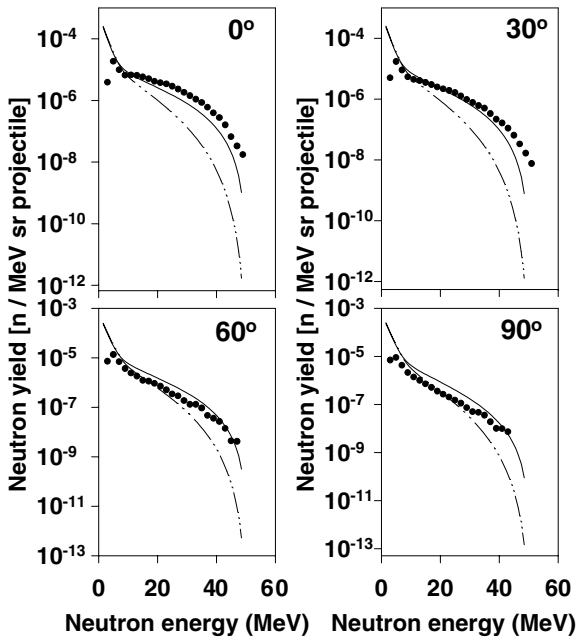

FIG. 5. Same as for Fig. 4 for 60-MeV α on Ta.

the emission angle θ and should be unity at 0° and zero at 90°. Thus, if $y^{\alpha}(\epsilon,\theta)$ be the angular distribution of emitted neutrons, then we propose to express it as follows:

$$y^{\alpha}(\epsilon,\theta) = b y^{\alpha}_{4,0}(\epsilon,\theta) + (1-b) y^{\alpha}_{5,1}(\epsilon,\theta), \tag{10}$$

where $y^{\alpha}_{4,0}(\epsilon,\theta)$ and $y^{\alpha}_{5,1}(\epsilon,\theta)$ are the number of neutrons emitted in a given direction θ with energy ϵ from 4p0h and 5p1h initial configurations, respectively, of α-induced reactions. Now, in Eq. (10), if we choose $b = \cos\theta$, then our calculation agrees well with available experimental data up to the 90° lab angle. For backward angles, this prescription is not valid. We have only 135°, backward-angle experimental data that appear to be comprised of evaporation neutrons only. Now Eq. (10) can be written as follows (valid for 0° to 90° angle):

$$y^{\alpha}(\epsilon,\theta) = y^{\alpha}_{4,0}(\epsilon,\theta)\cos\theta + y^{\alpha}_{5,1}(\epsilon,\theta)(1-\cos\theta) \tag{11}$$

In the next part of this work we obtained empirical expressions for the total neutron emission cross section as well as total neutron yield, energy distribution, and angular yield of neutrons from α-induced reactions on thick targets. As mentioned, we have used the results obtained from ALICE91 for 4p0h and 5p1h configurations and have mixed them as suggested by Gadioli *et al*. [8] to obtain the final expression for the neutron emission cross section. The empirical expressions for total, energy differential, and double differential (energy, angle) neutron yield distributions has been obtained separately for 4p0h and 5p1h initial configurations. Finally, to test the reliability of these empirical expressions, the angular distributions calculated using these relations are compared with experimentally measured data.

IV. FORMULATION OF EMPIRICAL EXPRESSIONS

A. Neutron emission cross section

Total neutron emission cross sections have been estimated for different elements ranging from ^{9}Be to ^{209}Bi for α-induced reactions for incident energy range 25–200 MeV. We have calculated the PEQ neutron energy spectra for α-induced reactions from Eq. (3) using the initial exciton numbers $n_0 = 4$ and $n_0 = 6$ separately and have estimated the energy integrated cross sections. The EQ neutron spectra are determined from Eq. (4) and the total (PEQ+EQ) energy integrated cross sections are calculated for all these target elements. To give proportionate weightage to the two types of reaction mechanisms we have taken 30% of the total neutron emission cross section calculated with $n_0 = 4$ and 70% of that with $n_0 = 6$ and added them together to get the final result.

This cross section is plotted against mass number in Fig. 6. The total neutron emission increases with target mass number A almost throughout the entire range of elements considered except for very high mass elements, as observed in our earlier study with protons [22]. The total neutron emission cross section is maximum around the mass number 175 for incident α energies of about 45 MeV and above. For lower incident α energies around 25 MeV a broad maximum occurs around the mass number 120. This cross section can be fitted with a third-degree polynomial in A (shown as solid lines in Fig. 6)

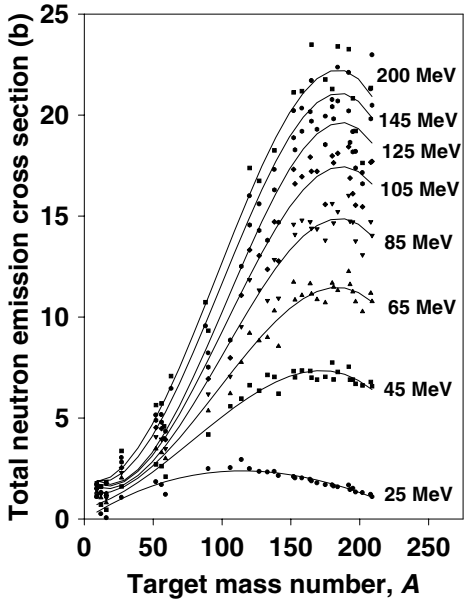

FIG. 6. Plot of the total neutron emission cross section against mass number A of target elements at different projectile energies ranging from 25 to 200 MeV. Symbols are the results from ALICE91, and the third-degree polynomial is shown by solid lines.

as follows:

$$\sigma^{\alpha}_{\text{emission}} = b^{\alpha}_0 + b^{\alpha}_1 A + b^{\alpha}_2 A^2 + b^{\alpha}_3 A^3. \tag{12}$$

Plots of b^{α}_i versus incident α energy E_{α} (Fig. 7) show a smoothly varying parabolic behavior for each of these

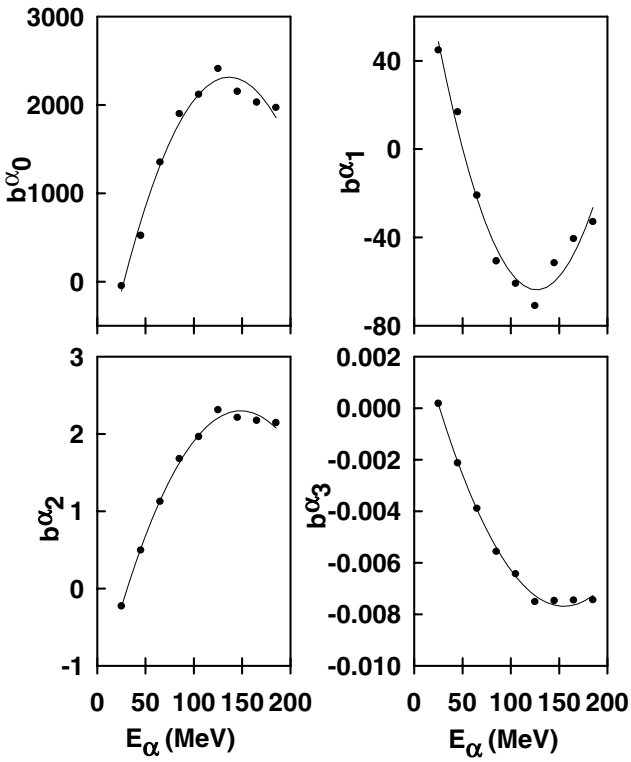

FIG. 7. Plot of coefficients b^{α}_0, b^{α}_1, b^{α}_2, and b^{α}_3 against incident projectile energy E_{α}.

TABLE I. Value of c_i^αs for different b_i^α's.

	b_0^α	b_1^α	b_2^α	b_3^α
c_0^α	1313.6044	110.9571	−1.3646	3.4479×10^{-3}
c_1^α	53.1883	−2.7606	0.0494	-1.4378×10^{-4}
c_2^α	−0.1949	0.0109	-1.6645×10^{-4}	4.6403×10^{-7}

coefficients with E_α. The coefficients b_0^α and b_2^α increase with incident α energy, reach a maximum at about 120 MeV, and then decrease slightly. The coefficients b_1^α and b_3^α, conversely, show a decreasing trend in increasing α energy to 120 MeV and then either increase (for b_1^α) or level off (for b_3^α). In analyzing these data we find that the coefficients b_i^α [Eq. (12)] can again be expressed as second degree polynomials in E_α:

$$b_i^\alpha = c_{i0}^\alpha + c_{i1}^\alpha E_\alpha + c_{i2}^\alpha E_\alpha^2. \tag{13}$$

The values of the coefficients c_{ij}^α that can be used to calculate the total neutron emission cross section in millibarn (mb) are listed in Table I.

B. Thick target neutron yield

We have calculated total neutron yield, energy spectrum, and angular distributions of neutrons from α-induced reactions on thick targets of same mass range from ^{9}Be to ^{209}Bi and for the same projectile energy range 25–200 MeV. We have used, for this purpose, the hybrid model code ALICE91 modified for thick targets.

1. Total neutron yield

Our calculated results show that the total neutron yield from thick targets increases with incident α energy (E_α) for each target element and the values of total neutron yield for the two initial configurations are very close. To ease our calculation of total neutron yield, we have, therefore, taken the weighted average yield from 4p0h (30%) and 5p1h (70%) configurations. From the plots of total neutron yield against incident α energies (Fig. 8) it has been observed that the slope of the curves changes around 100 MeV for all elements. Consequently, to facilitate the fitting procedure we have divided the incident α-energy range into two parts: $E_\alpha <$ 100 MeV and $E_\alpha \geqslant 100$ MeV. Figures 8(a) ($E_\alpha < 100$ MeV) and 8(b) ($E_\alpha \geqslant 100$ MeV) give plots of total neutron yield against incident α energies for different target masses. In each of these two different ranges, the total neutron yield obtained from ALICE91 can be fitted with second-degree polynomials as follows:

$$\begin{aligned} Y_{\text{tot}}^\alpha &= C_0^{\alpha A} + C_1^{\alpha A} E_\alpha + C_2^{\alpha A} E_\alpha^2 \\ &\quad \text{for } 25 \text{ MeV} \leqslant E_\alpha \leqslant 100 \text{ MeV} \\ &= C_0^{\prime\alpha A} + C_1^{\prime\alpha A} E_\alpha + C_2^{\prime\alpha A} E_\alpha^2 \\ &\quad \text{for } 100 \text{ MeV} \leqslant E_\alpha \leqslant 200 \text{ MeV}. \end{aligned} \tag{14}$$

The coefficients $C_i^{\alpha A}$ and $C_i^{\prime\alpha A}$ show systematic behavior with target mass (Fig. 9), and they are fitted in turn against

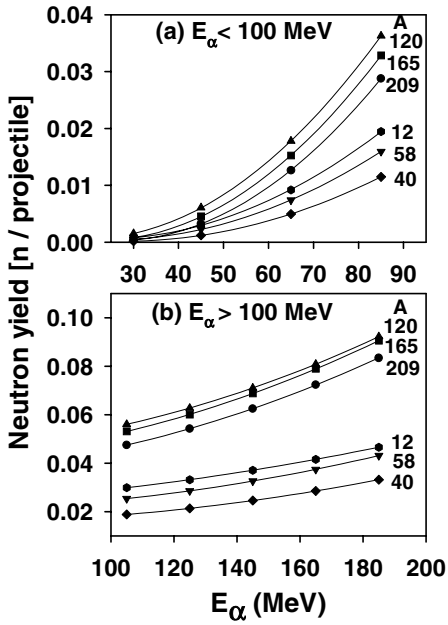

FIG. 8. Plot of total neutron yield versus α energy, E_α for different thick targets. The solid line represents the fitted curve through the ALICE91 calculations (symbols).

target mass numbers A using polynomials of the following type:

$$C_i^{\alpha A} = \sum_{j=0}^{j_{\max}} C_{ji}^{\alpha a} A^j. \tag{15}$$

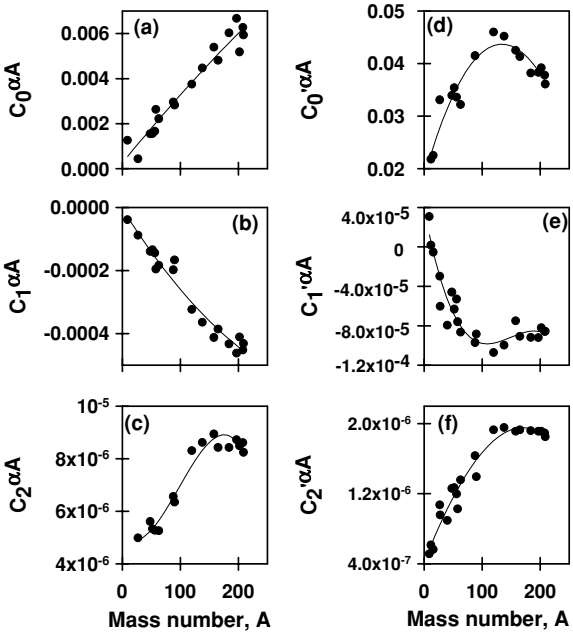

FIG. 9. Plot of $C_i^{\alpha A}$ and $C_i^{\prime\alpha A}$ against target mass number A. The solid line represents the fitted curve through the data (symbols). (a) for $C_0^{\alpha A}$, (b) for $C_1^{\alpha A}$, and (c) for $C_2^{\alpha A}$, each for $E_\alpha < 100$ MeV; and (d) for $C_0^{\prime\alpha A}$, (e) for $C_1^{\prime\alpha A}$, and (f) for $C_2^{\prime\alpha A}$, each for $E_\alpha \geqslant$ 100 MeV.

TABLE II. The values of the coefficients $C_{ji}^{\alpha a}$.

	i	$j=0$	$j=1$	$j=2$	$j=3$
$25 \leqslant E_\alpha < 100$ MeV	0	2.5966×10^{-4}	3.1552×10^{-5}	-1.3894×10^{-8}	0.0
	1	-3.9166×10^{-6}	-2.9256×10^{-6}	3.6759×10^{-9}	0.0
	2	5.1019×10^{-6}	-2.2060×10^{-8}	6.2354×10^{-10}	-2.1317×10^{-12}
$E_\alpha \geqslant 100$ MeV	0	0.0184	3.9143×10^{-4}	-1.6076×10^{-6}	7.2871×10^{-10}
	1	3.8546×10^{-5}	-3.1106×10^{-6}	2.2475×10^{-8}	-5.0166×10^{-11}
	2	4.1974×10^{-7}	1.6773×10^{-8}	-3.8483×10^{-11}	-4.1473×10^{-14}

It is observed that for the energy range 25–100 MeV Eq. (15) becomes a second-degree polynomial (e.g., $j_{\max} = 2$ for $i = 0, 1$), whereas for all other cases $j_{\max} = 3$. The values of the coefficients $C_{ji}^{\alpha a}$ are listed in Table II for the two different E_α ranges as described above.

2. *Differential energy spectrum*

To obtain an empirical relation of the energy differential neutron yields from thick target, we have adopted the following procedures:

(i) The incident α energy range is divided in two regions: 25 MeV $\leqslant E_\alpha <$ 100 MeV, and $E_\alpha \geqslant$ 100 MeV.
(ii) The neutron emission energy ϵ is divided by the incident α energy E_α to define a new dimensionless variable ϵ/E_α.
(iii) The energy differential neutron yield $y^\alpha(\epsilon)$ is divided by the total neutron yield Y_{tot}^α and then $y^{\alpha R}(\epsilon) = [y^\alpha(\epsilon)/Y_{\text{tot}}^\alpha]A^w$ is taken as the dependent variable to be fitted against ϵ/E_α. Here, A is the mass number and w is a fractional parameter, whose value depends on the range of ϵ.
(iv) The emission energy range ϵ is divided in two regions, $\epsilon/E_\alpha \leqslant 0.05$ and $\epsilon/E_\alpha > 0.05$. The lower part of the emission energy is assumed to be composed mainly of evaporation neutrons, whereas the upper part is assumed to be composed mainly of PEQ emissions. We have taken for $\epsilon/E_\alpha \leqslant 0.05$, $w = 0$, whereas for $\epsilon/E_\alpha > 0.05$, $w = 0.6$.

For ($0 \leqslant \epsilon/E_\alpha \leqslant 0.05$)

In this case the following expression similar to that used for emissions from the evaporation process is chosen as follows:

$$y^{\alpha R}(\epsilon) = C^{\alpha W} \epsilon \exp(-\epsilon/T^\alpha). \tag{16}$$

In Eq. (16) the parameters $C^{\alpha W}, T^\alpha$ are found to be functions of mass number A and can be expressed as follows:

$$C^{\alpha W} = \sum_{i=0}^{2} K_i^\alpha A^i \tag{17}$$

and

$$T^\alpha = \sum_{i=0}^{3} l_i^\alpha A^i, \tag{18}$$

where K_i^αs and l_i^αs can be expressed as a second-degree polynomial in E_α as follows:

$$K_i^\alpha = \sum_{j=0}^{2} C_{ji}^{\alpha WC} E_\alpha^j \tag{19}$$

and

$$l_i^\alpha = \sum_{j=0}^{2} C_{ji}^{\alpha WT} E_\alpha^j. \tag{20}$$

The values of $C_{ji}^{\alpha WC}$ and $C_{ji}^{\alpha WT}$ are listed in Tables III and IV, respectively.

TABLE III. The values of the coefficients $C_{ji}^{\alpha WC}$.

		i	$j=0$	$j=1$	$j=2$
$25 \leqslant E_\alpha < 100$ MeV	4p0h	0	0.5876	−0.0108	6.5128×10^{-5}
		1	0.0121	-6.1758×10^{-5}	-1.6843×10^{-7}
		2	1.6205×10^{-5}	-7.0498×10^{-7}	5.8366×10^{-9}
	5p1h	0	0.4230	-4.5651×10^{-3}	1.0529×10^{-5}
		1	0.0177	-2.5193×10^{-4}	1.3611×10^{-6}
		2	-4.1054×10^{-6}	-4.7336×10^{-9}	-1.3490×10^{-11}
$E_\alpha \geqslant 100$ MeV	4p0h	0	0.2554	-2.3019×10^{-3}	5.4261×10^{-6}
		1	5.9660×10^{-3}	2.2879×10^{-6}	-2.6988×10^{-8}
		2	-6.4298×10^{-6}	4.0587×10^{-8}	-2.2890×10^{-10}
	5p1h	0	l0.1889	-1.4229×10^{-3}	2.6483×10^{-6}
		1	6.6571×10^{-3}	-8.5387×10^{-6}	1.9644×10^{-9}
		2	-7.1914×10^{-6}	4.0514×10^{-8}	-2.1036×10^{-10}

TABLE IV. The values of the coefficients $C_{ji}^{\alpha WT}$.

		i	$j=0$	$j=1$	$j=2$
$25 \leqslant E_\alpha < 100$ MeV	4p0h	0	1.1522	-4.0428×10^{-3}	1.4839×10^{-4}
		1	−0.0108	3.1887×10^{-4}	-4.3604×10^{-6}
		2	4.8285×10^{-5}	-2.2133×10^{-6}	3.1546×10^{-8}
		3	-6.8192×10^{-8}	4.5412×10^{-9}	-7.0641×10^{-11}
	5p1h	0	1.1383	7.0292×10^{-3}	9.0680×10^{-5}
		1	−0.0108	-1.9631×10^{-5}	-2.3921×10^{-6}
		2	4.7316×10^{-5}	8.1118×10^{-7}	1.3396×10^{-8}
		3	-6.3661×10^{-8}	-3.4307×10^{-9}	-2.1911×10^{-11}
$E_\alpha \geqslant 100$ MeV	4p0h	0	0.3227	0.0203	-2.3835×10^{-5}
		1	0.0178	-4.1452×10^{-4}	3.8054×10^{-7}
		2	-1.4289×10^{-4}	2.8390×10^{-6}	-1.6968×10^{-9}
		3	3.3845×10^{-7}	-6.4836×10^{-9}	3.0021×10^{-12}
	5p1h	0	0.8652	0.0223	-3.2984×10^{-5}
		1	1.8462×10^{-3}	-4.6161×10^{-4}	6.3207×10^{-7}
		2	-8.6969×10^{-6}	3.2354×10^{-6}	-3.7792×10^{-9}
		3	8.8631×10^{-9}	-7.6365×10^{-9}	8.6820×10^{-12}

For ($\epsilon/E_\alpha > 0.05$)

For this emission energy range, the expression for $y^{\alpha R}(\epsilon)$ is taken as follows:

$$\log[y^{\alpha R}(\epsilon)] = \sum_{i=0}^{3} C_i^{\alpha P} (\epsilon/E_\alpha)^i, \tag{21}$$

where for calculating $y^{\alpha R}(\epsilon)$ we have taken $w = 0.6$. In this case also we could obtain a polynomial expression for $C_i^{\alpha P}$ in terms of the incident α energy E_α as follows:

$$C_i^{\alpha P} = \sum_{j=0}^{j_{\max}} C_{ji}^{\alpha PE} E_\alpha^j. \tag{22}$$

Here, $j_{\max} = 2$ for $E_\alpha < 100$ MeV and $j_{\max} = 3$ for $E_\alpha \geqslant 100$ MeV. The values of $C_{ji}^{\alpha PE}$s are listed in Table V.

3. Double differential energy spectrum

Angular distributions of the energy differential neutron yield have been calculated by the following:

$$y^\alpha(\epsilon, \theta) = \frac{y_{4,0}^\alpha(\epsilon)\cos\theta + y_{5,1}^\alpha(\epsilon)(1-\cos\theta)}{4\pi} \frac{a}{\sinh(a)} \times [\cosh(a\cos\theta) + \sinh(a\sin\theta)], \tag{23}$$

where the a parameter is dependent on ϵ as follows [15]:

$$a = 0.04\epsilon + 1.8206 \times 10^{-6}\epsilon^3 + 6.652428 \times 10^{-9}\epsilon^4. \tag{24}$$

TABLE V. The values of the coefficients $C_{ji}^{\alpha PE}$.

		i	$j=0$	$j=1$	$j=2$	$j=3$
$25 \leqslant E_\alpha < 100$ MeV	4p0h	0	1.0508	-1.7987×10^{-3}	-7.4375×10^{-5}	0.0
		1	−1.8955	−0.3137	2.3122×10^{-3}	0.0
		2	−17.3375	1.1652	-8.0735×10^{-3}	0.0
		3	13.7636	−0.9814	6.8406×10^{-3}	0.0
	5p1h	0	2.4824	−0.0298	9.5508×10^{-5}	0.0
		1	−18.4503	0.0104	3.3756×10^{-4}	0.0
		2	31.0687	0.1085	-1.5029×10^{-3}	0.0
		3	−39.9412	0.1823	-4.0067×10^{-4}	0.0
$E_\alpha \geqslant 100$ MeV	4p0h	0	10.5220	−0.2085	1.3521×10^{-3}	-2.9198×10^{-6}
		1	−129.4199	2.4602	−0.0165	3.5977×10^{-5}
		2	394.6851	−7.6644	0.0508	-1.0927×10^{-4}
		3	−312.5591	5.9613	−0.0390	8.3271×10^{-5}
	5p1h	0	3.3729	−0.0543	3.4372×10^{-4}	-7.7776×10^{-7}
		1	−47.8688	0.7211	-5.3079×10^{-3}	1.2453×10^{-5}
		2	201.4530	−3.6027	0.0249	-5.5281×10^{-5}
		3	−193.3755	3.3794	−0.0226	4.8975×10^{-5}

Here, $y^{\alpha}_{4,0}(\epsilon)$ and $y^{\alpha}_{5,1}(\epsilon)$ are the energy differential neutron yield for 4p0h and 5p1h configurations, respectively, and can be evaluated as follows:

$$y^{\alpha}_{p,h}(\epsilon) = y^{\alpha R}_{p,h}(\epsilon) Y^{\alpha}_{\rm tot} A^{-w}, \tag{25}$$

where $Y^{\alpha}_{\rm tot}$ can be estimated using Eq. (14) and $y^{\alpha R}_{p,h}(\epsilon)$ can be calculated with help of Eqs. (16)–(21). Here (p, h) stands for either (4,0) or (5,1) initial configurations. Equation (23) is the final expression that can be used to calculate double differential neutron yield distributions from α-induced reactions on thick targets.

V. RESULTS AND DISCUSSION

A. Neutron emission cross section

From the analysis of total neutron emission cross sections from various target elements in α-induced reaction it is seen (Fig. 6) that the total neutron emission cross section increases with target mass number. This trend is similar to that in the case of proton-induced reactions in this energy range [22]. From a comparison of the results of our empirical formulation with ALICE91 calculation it is seen that, except in the case of ^{12}C and ^{16}O, the percentage deviation in the total neutron yield calculated using the empirical relation is less than 15% as compared to the calculations of ALICE91. We could make the comparison only with calculated results from a code in the absence of sufficient reliable experimental data of neutron emission cross sections from α-induced reactions. Thus it can be concluded that the empirical formula given by Eq. (12) reproduces the total neutron emission cross sections with reasonable accuracy over the entire mass range.

1. Trends in neutron emission cross section in α-induced reaction

To understand the mechanism of neutron emission from α-induced reactions we have studied the PEQ and EQ neutron multiplicities, which are defined as follows:

$$\begin{aligned} N_{\rm PEQ} &= \frac{\sigma^{\alpha}_{\rm PEQ}}{\sigma^{\alpha}_{\rm abs}} \\ N_{\rm EQ} &= \frac{\sigma^{\alpha}_{EQ}}{\sigma^{\alpha}_{\rm abs}}. \end{aligned} \tag{26}$$

The PEQ and EQ neutron multiplicities for 45 and 85 MeV incident α energy are plotted against mass number A (Figs. 10 and 11, respectively) for both the initial configurations $n_0 = 4$ and $n_0 = 6$ in each case. It is seen from Fig. 10 that PEQ neutron emission cross section is considerably larger for the initial configuration 4p0h ($n_0 = 4$) compared to 5p1h ($n_0 = 6$) for the entire mass range.

This can be explained from the fact that when we consider $n_0 = 4$, PEQ emission starts from $n_0 = 4$, which is one stage earlier than that for $n_0 = 6$. Although ALICE91 uses "never come back" approximation, 4p0h initial configuration has additional contributions from the stage $n_0 = 4$ over $n_0 = 6$. Moreover PEQ emission probability is larger in the earlier stage of reaction because excitation energy is shared among fewer particles.

Our investigation reveals that the EQ (Fig. 11) as well as the total neutron emission cross section is larger for 5p1h

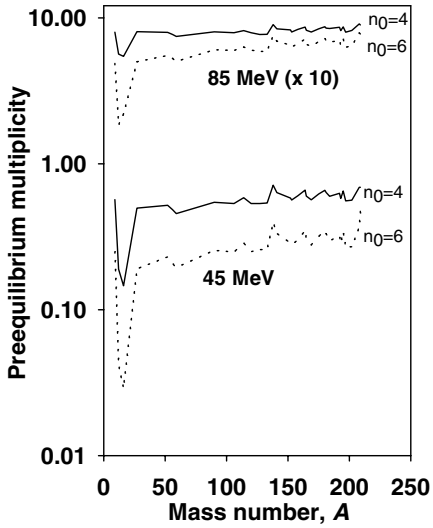

FIG. 10. Plot of PEQ neutron multiplicity against mass number of target elements, A for $n_0 = 4$ and 6 initial configurations.

configuration than the other case. This can be explained as follows: Because PEQ emission is larger for $n_0 = 4$, residual excitation is less in this case than that for $n_0 = 6$. From Eq. (4) we see that EQ emission depends exponentially on the excitation energy of the residual nucleus. As a result, the EQ neutron emission is larger for the $n_0 = 6$ than for the $n_0 = 4$ configuration. Because the EQ emission dominates the total neutron emission cross section in the energy range considered, the total neutron emission cross section is larger for the 5p1h initial configuration for all the target elements considered. From Figs. 10 and 11 it is seen that there is a sharp drop in the PEQ and EQ neutron emissions around the target element ^{16}O.

The total neutron emission cross section for all incident α energies increases initially with mass number and then

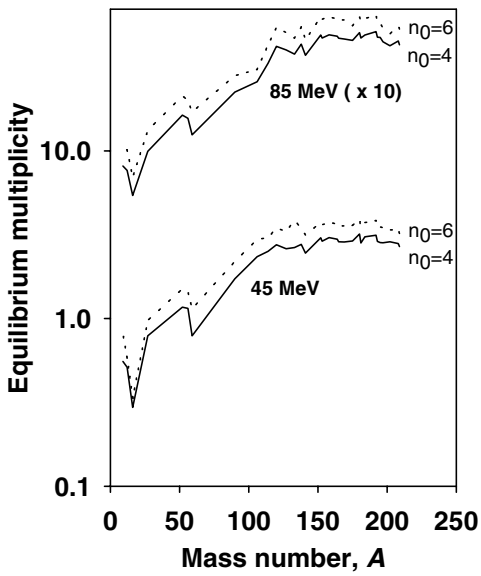

FIG. 11. EQ neutron multiplicity plotted against mass number, A for $n_0 = 4$ and 6 initial configurations.

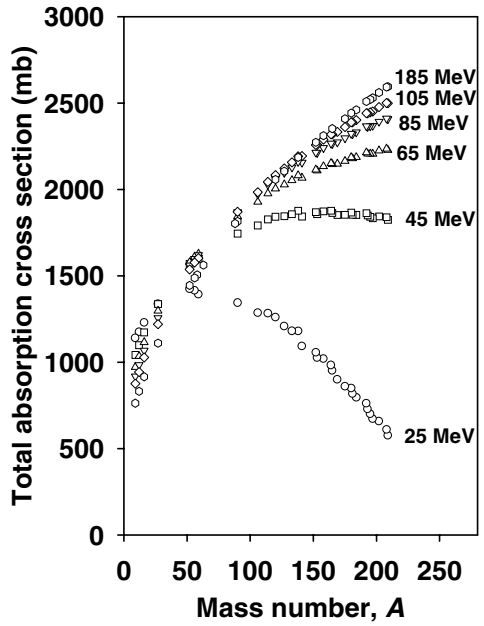

FIG. 12. Plot of total absorption cross section for the α projectile against mass number A at different E_α.

decreases. This trend is similar to that for $\sigma_{\rm abs}$ for different nuclei (Fig. 12). However, for higher incident α energies the slight decrease at larger masses is because of the decrease in EQ neutron emission multiplicity, which dominates the total neutron multiplicity. The reduced neutron emission is observed in ^{202}Hg, ^{197}Au, and ^{208}Pb with maximum reduction for ^{202}Hg. It is observed that α-emission cross sections are significantly higher in these nuclei compared to those in the neighboring

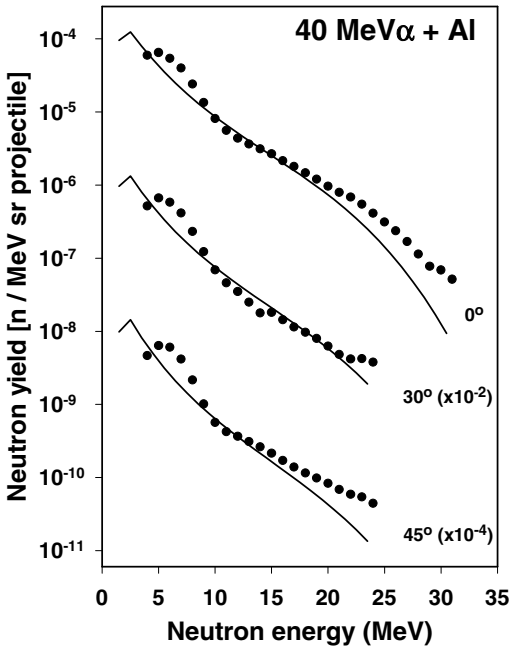

FIG. 13. Comparison of measured neutron yield for 40 MeV α on Al [9] (symbols) with calculated (lines) results at 0°, 30°, and 45° lab angles. Error bars are shown when they exceed the symbol size.

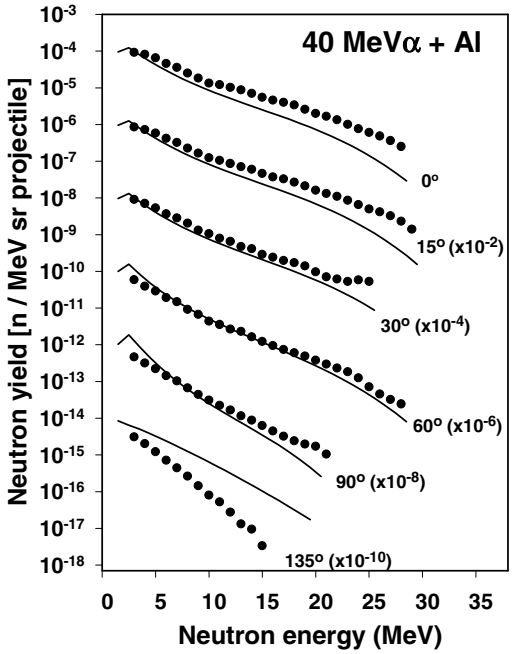

FIG. 14. Comparison of measured neutron yield for 40-MeV α on Al [21] (symbols) with calculated (lines) results at 0°, 15°, 30°, 60°, 90°, and 135° lab angles.

nuclei. This reduces competitively the neutron emission cross sections in these three nuclei. At larger target masses the total excitation caused by the incident α is shared by larger number of nucleons, thereby reducing the energy per nucleon and the emission probability.

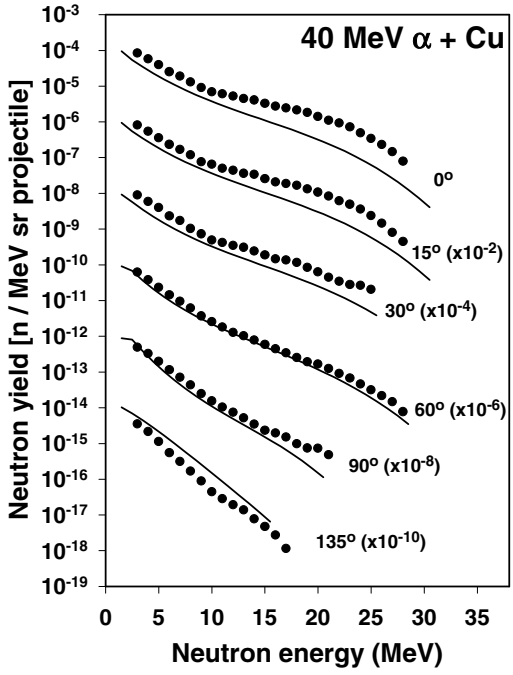

FIG. 15. Same as Fig. 14 for 40-MeV α on Cu.

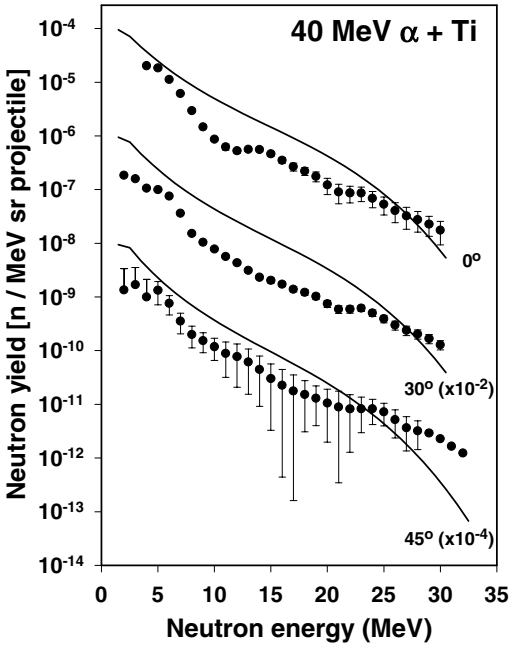

FIG. 16. Comparison of measured neutron yield for 40-MeV α on Ti [9] (symbols) with calculated (lines) results at 0°, 30°, and 45° lab angles. Error bars are shown when they exceed the symbol size.

B. Thick target

We have compared the experimentally measured angular distribution of neutrons from thick targets with the results of ALICE91 calculated using the two different initial configurations. Our analysis shows that for 40-MeV α-induced reaction the neutron emission at forward angles (0°, 15°, and 30°) are very well predicted by the 4p0h initial configuration for Al and Cu targets (Figs. 1 and 2) [21]. As we move to back angles the 5p1h configuration plays the dominant role. But at 135° emission angle neutrons are mainly contributed by evaporation and both choices for PEQ emission overpredict the measured data. For 40-MeV α on Pb [21] (Fig. 3) the forward angle emissions (up to 30°) are underpredicted by

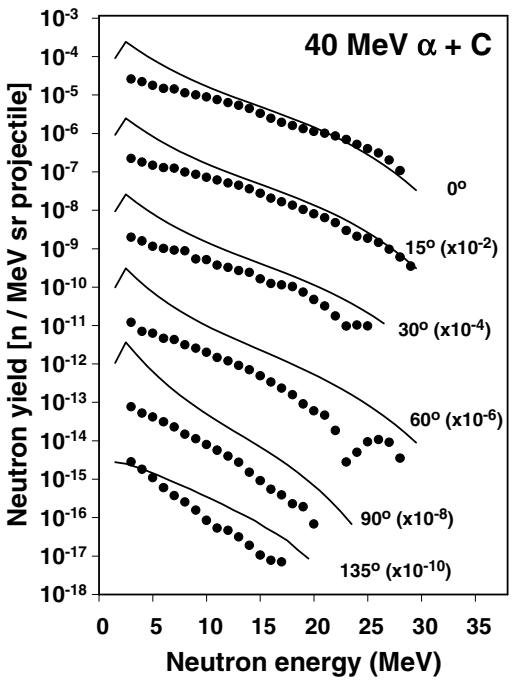

FIG. 17. Same as Fig. 14 for 40 MeV α on C.

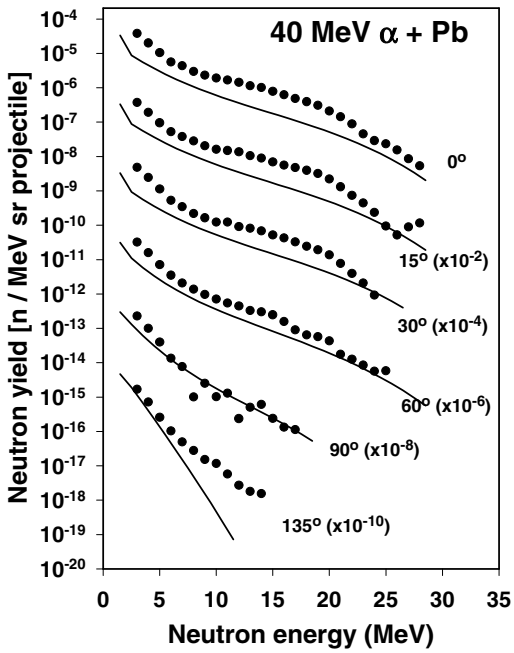

FIG. 18. Same as Fig. 14 for 40-MeV α on Pb.

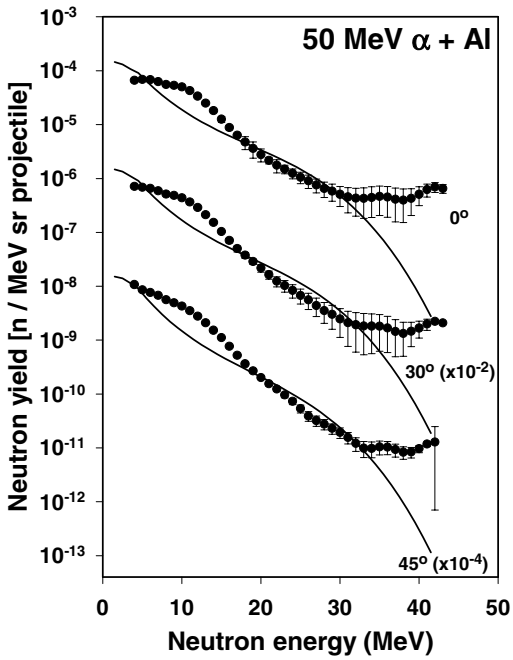

FIG. 19. Comparison of measured neutron yield for 50-MeV α on Al [9] (symbols) with calculated (lines) results at 0°, 30°, and 45° lab angles. Error bars are shown when they exceed the symbol size.

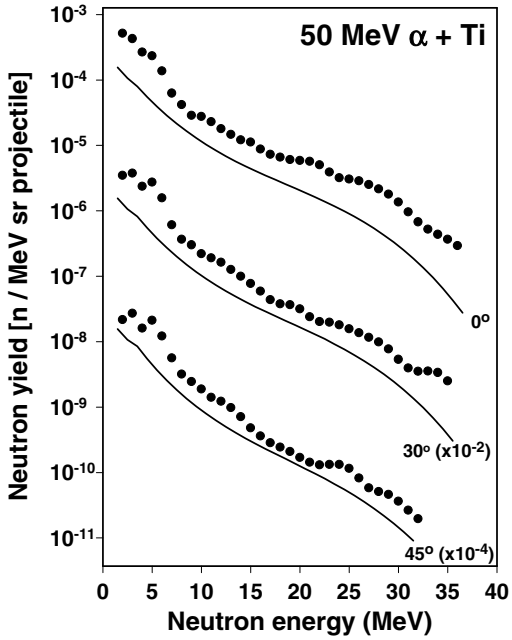

FIG. 20. Comparison of measured neutron yield for 50-MeV α on Ti [9] (symbols) with calculated (lines) results at 0°, 30°, and 45° lab angles. Error bars are shown when they exceed the symbol size.

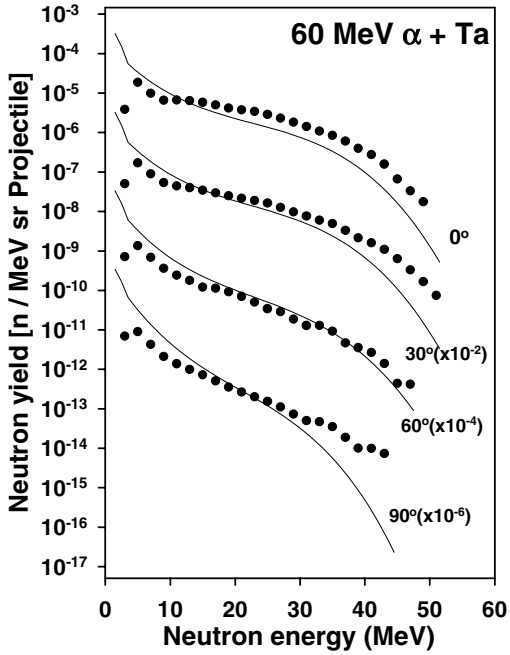

FIG. 22. Comparison of measured neutron yield for 60-MeV α on Ta [20] (symbols) with calculated (lines) results at 0°, 30°, 60°, and 90° lab angles.

both 4p0h and 5p1h configuration, but the 4p0h distributions are closer to the experimental data. At 60° emission angle the neutron distribution is fairly well reproduced by the 4p0h calculations. At backward angles the 5p1h calculations show better agreement with the measured data. Figures 4 and 5 show the comparison in the case of 50- and 60-MeV

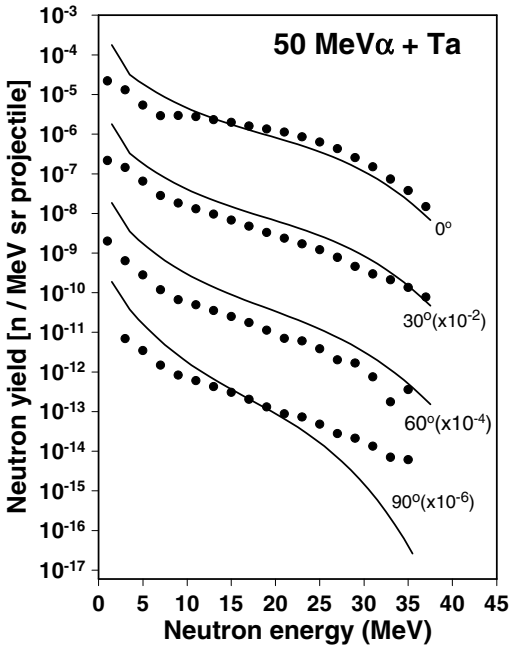

FIG. 21. Comparison of measured neutron yield for 50-MeV α on Ta [20] (symbols) with calculated (lines) results at 0°, 30°, 60°, and 90° lab angles.

α-induced reactions on Ta. It is seen that for 50-MeV projectile energy, neutron emission at 0° is very well predicted by the 4p0h configuration. But as we go to backward angles (e.g., 30°, 60°, and 90°) the 4p0h configuration overpredicts the measured distrbution more and more. At 90° emission angle the angular distribution is solely given by the emission from 5p1h configuration along with evaporation. It is seen that at large values of target mass A and at forward directions, even though the agreement between the exponential data and the 4p0h emission is better than that from 5p1h configuration, the emissions are slightly underestimated by 4p0h configuration. Our study showed that an weighted sum of the emissions from the two initial configuration can predict the measured distribution better. The weighting factors are found to be $\cos\theta$ for 4p0h and $(1 - \cos\theta)$ for 5p1h.

The emissions from the 4p0h state can be considered as those from direct reactions. Such a conclusion has also been made by Grimes *et al*. [23]. This explains the predominance of 4p0h initial configuration in the forward angle emissions with gradually decreasing contributions at larger angles. However, it may be noted that emissions from 4p0h initial configuration also contain subsequent emissions from 5p1h and higher exciton states. This explains the fact that emissions from the 4p0h initial configuration is less forward peaked than expected from a pure direct reaction.

To test the validity of our empirical formula in predicting angular distributions of thick target neutron yield from α-induced reactions, we have compared our calculated results with available experimental data. Experimentally measured neutron angular distribution [9,20,21] for 40-MeV α incident on Al, Ti, Cu, C, and Pb as well as 50-MeV α on Al and Ti and 50- and 60-MeV α on Ta have been compared with the results

of our calculations. Comparisons have been made at different emission angles ranging from 0° to a maximum of 135°. Figures 13–22 show the plots of those comparisons. In general the calculated angular distribution is fairly well reproduced for Al, Cu targets [27] (Figs. 13–15). For Ti (Fig. 16) [9] we see that our calculations overpredict the experimental data to some extent. In the case of the C target (Fig. 17) the forward angle distribution is well predicted by our calculations, whereas the backward-angle neutron emission is overpredicted. For the Pb target [21] (Fig. 18) the overall agreement between the calculated and the experimental data is satisfactory; the forward angle emissions being slightly underpredicted. At backward angles the measured data are well reproduced by the calculated distribution, the contribution of 5p1h initial configuration being more dominant as the emission angle increases. For 50-MeV α on Al [9] (Fig. 19), Ti [9] (Fig. 20), and Ta [20] (Fig. 21), we see that our calculations more or less agree with experimental data except for some discrepancies at high emission energies. In case of 60-MeV α on Ta [20] (Fig. 22) also we have good agreement between calculation and experiment. From the study of neutron energy-angle distribution for α-induced reaction it has been observed that the empirical formula reported in this work predicts the measured distribution more or less accurately.

VI. SUMMARY AND CONCLUSIONS

We have analyzed the trend of neutron emission from α-induced reactions on various target elements and have obtained empirical expressions to describe emission cross section, total yield, and energy as well as angular distribution of neutron yield from thick targets. The parameters of the functional fits to the total neutron yield, neutron energy spectra and angular distribution calculated by ALICE91 are given in the tables. Using these parameter values and with the help of Eqs. (14)–(24) one can obtain total yield, emitted energy distribution, and angular distribution of neutrons. These empirical relations would be very useful in quick calculations of the shielding and other safety designs in particle accelerators. We have also shown that neutron emissions from the two initial configurations 4p0h and 5p1h differ in angular distributions with the former being more forward peaked. Our analysis supports the assumption that emissions from the 4p0h exciton configuration are a result of direct reaction mechanism.

ACKNOWLEDGMENT

This work has been carried out as a part of a project (No. AERB/20/04) sponsored by the Atomic Energy Regulatory Board, India.

[1] C. Mayer-Böricke, Nukleonika **22**, 1131 (1977).
[2] G. Chenevert, N. S. Chant, I. Halpern, G. Glashausser, and D. L. Hendrie, Phys. Rev. Lett. **27**, 434 (1971).
[3] R. W. Koontz, C. C. Chang, H. D. Holmgren, and J. R. Wu, Phys. Rev. Lett. **43**, 1862 (1979).
[4] J. R. Wu, C. C. Chang, H. D. Holmgren, and R. W. Koontz, Phys. Rev. C **20**, 1284 (1979).
[5] H. D. Holmgren, C. C. Chang, R. W. Koontz, and J. R. Wu, in *Proceedings of the Second International Conference on Nuclear Reaction Mechanisms, Varenna, 1979* (University of Milano, Milano, 1979).
[6] M. Blann, Annu. Rev. Nucl. Sci. **25**, 123 (1975), and references therein.
[7] E. Gadioli, Nukleonika **21**, 385 (1976), and references therein.
[8] E. Gadioli and E. Gadioli-Erba, Z. Phys. A **299**, 1 (1981).
[9] D. Dhar, S. N. Roy, T. Bandyopadhyay, and P. K. Sarkar, Phys. Rev. C **67**, 024607 (2003).
[10] M. Maiti, M. Nandy, S. N. Roy, and P. K. Sarkar, Nucl. Instr. Meth. Phys. Res. B **215**, 317 (2004).
[11] T. Kota and T. Nakamura, Nucl. Instr. Meth. Phys. Res. A **311**, 548 (1992).
[12] M. Blann, Phys. Rev. Lett. **27**, 337 (1971); **27**, 700(E) (1971); **27**, 1550 (E) (1971); Nucl. Phys **A213**, 570 (1973).
[13] M. Blann, Lawrence Livermore National Laboratory Report No. UCID 19614 (1982); M. Blann, International Centre for Theoretical Physics Workshop on Applied Nuclear Theory and Nuclear Model Calculations for Nuclear Technology Applications, Trieste, Italy, SMR/284-1, 1988.
[14] M. Blann and H. K. Vonach, Phys. Rev. C **28**, 1475 (1983).
[15] C. Kalbach, Phys. Rev. C **37**, 2350 (1988).
[16] J. F. Ziegler, J. P. Biersack, and U. Littmark, *The Stopping and Range of Ions in Solids* (Pergamon Press, New York, 1985).
[17] T. Nakamura and Y. Uwamino, Phys. Rev. C **29**, 1317 (1984).
[18] N. L. Singh, J. Phys. G: Nucl. Part. Phys. **18**, 927 (1992).
[19] M. Cronqvist, S. Mattsson, M. Rydehell, O. Skeppstedt, S. E. Arnell, and L. Westerberg, Physica **39** (5), 547 (1973).
[20] P. K. Sarkar, T. Bandyopadhyay, G. Muthukrishnan, and S. Ghosh, Phys. Rev. C **43**, 1855 (1991).
[21] K. Shin, K. Miyahara, E. Tanabe, and Y. Uwamino, Nucl. Sci. Eng., **120**, 40 (1995).
[22] M. Maiti, M. Nandy, S. N. Roy, and P. K. Sarkar, Pramana J. Phys. **60** (1), 143 (2003).
[23] S. M. Grimes, J. D. Anderson, J. W. McClure, B. A. Pohl, and C. Wong, Phys. Rev. C **3**, 645 (1971).